Electronic supplementary information

Anion Amphiprotic Ionic Liquids as Protic Electrolyte Matrices allowing Sodium Metal Plating

Piotr Jankowski,[a,b,c*] Karolina Matuszek,[d] Marcel Treskow,[a,e] Michel Armand,[f] Douglas MacFarlane,[d] Patrik Johansson[a,g]

[a] Chalmers University of Technology, Department of Physics, 412 96 Gothenburg, Sweden

[b] Technical University of Denmark, Department of Energy Conversion and Storage, 2800 Kgs. Lyngby, Denmark

[c] Warsaw University of Technology, Faculty of Chemistry, 00-664 Warsaw, Poland

[d] Monash University, School of Chemistry, 3800 Clayton, Victoria, Australia

[e] Current address: Evonik R&D, Frankfurt am Main, Germany

[f] CIC Energigune, 01510 Miñano, Spain

[g] Alistore – European Research Institute, CNRS FR 3104, Hub de l'Energie, 15 Rue Baudelocque, 80039 Amiens, France

*pioja@dtu.dk

Experimental part

1. Synthesis of [EMIm][TFSAm]

[EMIm][TFSAm] was obtained from a two-step reaction. First, a solution of 1-ethyl-3-methylimidazolium chloride ([EMIm]Cl, Sigma-Aldrich, 5.36 g) in water ((≈15 g) was slowly passed through a column packed with Amberlite A26 (Sigma-Aldrich, 60g), in order to obtain 1-ethyl-3-methylimidazolium hydroxide ([EMIm][OH]). To ensure complete anion exchange, the column was further washed with water until the filtrate changed pH from alkaline to neutral. To the obtained solution of [EMIm][OH] (yield=94.7%, determined by potentiometric titration), an equimolar amount of trifluoromethanesulfonamide (TFSAmH, Sigma-Aldrich, 5.20 g) was added and the solution intensively stirred at room temperature under reflux overnight. Subsequently, the solvent was removed from the reaction mixture with a rotary evaporator at 60 ^{o}C and 50 mbar, giving a yellow oil containing [EMIm][TFSAm]. The crude product was purified using a column containing activated charcoal (Sigma-Aldrich), silica gel (Sigma-Aldrich), activated aluminium oxide (Sigma-Aldrich), and methanol as an eluent. The eluate was collected and concentrated with a rotary evaporator at 50 ^{o}C and 50 mbar leaving a yellowish oil of [EMIm][TFSAm] (8.80 g, yield = 97.3%). The product structure was confirmed with NMR and mass spectroscopies (Figures S1-S3).

2. Materials preparation and characterization

The [EMIm][TFSAm] and [EMIm][HSO_4] (Sigma-Aldrich, >95%) were both dried under vacuum at 90 ^{o}C for 24 h and subsequently moved to an Ar glovebox (H_2O <1 ppm, O_2 <10 ppm) without any exposure to air. The water content was assessed by Karl-Fisher titration (Metrohm 831 KF Coulometer) to be <45 and <30 ppm for [EMIm][TFSAm] and [EMIm][HSO_4], respectively. Electrolytes were prepared by direct mixing of the appropriate amount of the IL and NaTFSI (Solvionic, 99.5%) and heating the mixture to 100 ^{o}C under magnetic stirring until homogeneous.

The viscosities were measured using a Lovis 2000 M/ME (Anton Paar) operating between 10 - 80 ^{o}C using a 2.5 mm diameter capillary filled with the sample and a steel ball. The ionic conductivities were measured using a Novocontrol broad-band dielectric spectrometer in the frequency range 10^{-1}–10^{7} Hz and in the temperature range of −60 ^{o}C - +120 ^{o}C with a step of 10 ^{o}C. The sample was placed between two stainless steel electrodes separated by a Teflon spacer inside a coin cell. The thermal data were recorded on a DSC250 (TA instruments) differential scanning calorimeter in the temperature range -150 ^{o}C - +200^{o}C. A few mg of each sample was placed in a hermetically sealed aluminium pan inside the glove-box. All measurements were made using a scan rate of 10 ^{o}C min^{-1} in the sequence cooling-heating-cooling – and the heating traces are reported. The Raman spectra were collected on a Nicolet Almega Raman dispersive spectrometer using a diode laser with a 532 nm excitation line and a spectral resolution of *ca.* 2 cm^{-1}. The FT-IR spectra were collected on a Bruker Alpha, using an ATR accessory with a diamond crystal and a spectral resolution of *ca.* 2 cm^{-1}.

The electrochemical and battery tests were performed using a VMP3 potentiostat (Bio-Logic). The electrochemical stability was tested in 3-electrode Swagelok cells with a Pt disc as the working electrode (WE) and an Ag wire as the reference electrode (RE). To calibrate the potential of the Ag wire a small amount of ferrocene was added to the AAILs and the potential

of Fc^+/Fc recorded *vs*. the Ag wire. The plating/stripping tests were performed in 2-electrode Swagelok cells with the sample placed between two sodium discs (Sigma-Aldrich) and the cell put in a temperature-controlled chamber (Pol-Eko) at 60 ^oC.

3. Computational studies

All DFT calculations were performed using M06-2X functional and 6-311++G(d,p) basis set, as implemented in Gaussian 16.[1] Interaction energies inside clusters were calculated in gas phase as a difference in electronic energy between separated ions and cluster, all related to optimized geometries. At least ten starting geometries was considered for each stoichiometry, results for the lowest energy clusters are presented. For the calculation of reduction potentials, the effect of solvent was modelled using the conductor-like polarizable continuum model (C-PCM) with water parametrization, and calculated according to a previously developed methodology.[2] The MD simulations were performed using the GROMACS package[3] with the OPLS-based force field. Parameters for Na^+, $[EMIm]^+$ and $[TFSI]^-$ were taken from the literature,[4–6] and for $[TFSAm]^-$ created by taking bonding parameters from $[TFSI]^-$, and adjusting non-bonding parameters to reproduce interactions from the DFT calculations (Table S1), using charges from NPA (Natural Population Analysis) scheme. The force field was validated by density evaluation, resulting in an error <1% (calc: 1.370 g/cm^3; exp: 1.382 g/cm^3). Using the random algorithm implemented in GROMACS seven systems were created: $(NaTFSI)_x([EMIm][TFSAm])_{1-x}$ (x=0; 0.1; 0.2; 0.3; 0.4; 0.5; 0.6), each containing in total 100 ion pairs. All systems were subsequently submitted to energy minimization and simulations under NVT and NPT conditions to obtain the starting geometries, followed by equilibration at 303 K for 10 ns. The MD production runs were 50 ns long using a time step of 2 fs and a leapfrog algorithm under NPT and periodic boundary conditions at 1 bar and a V-rescale thermostat (coupling time 0.5 ps) and a Parrinello–Rahman barostat (coupling time 2 ps). A particle-mesh Ewald summation routine was used for the long-range forces (cut-off 12 Å). The SHAKE algorithm was used to constrain bonds involving hydrogen. The analysis of trajectories was performed using tools implemented in the GROMACS package: composition of the coordination shells (coordination numbers) were obtained from radial distribution functions (rdf); diffusion coeficients were obtained from Einstein relation using MSD-generated mobility.

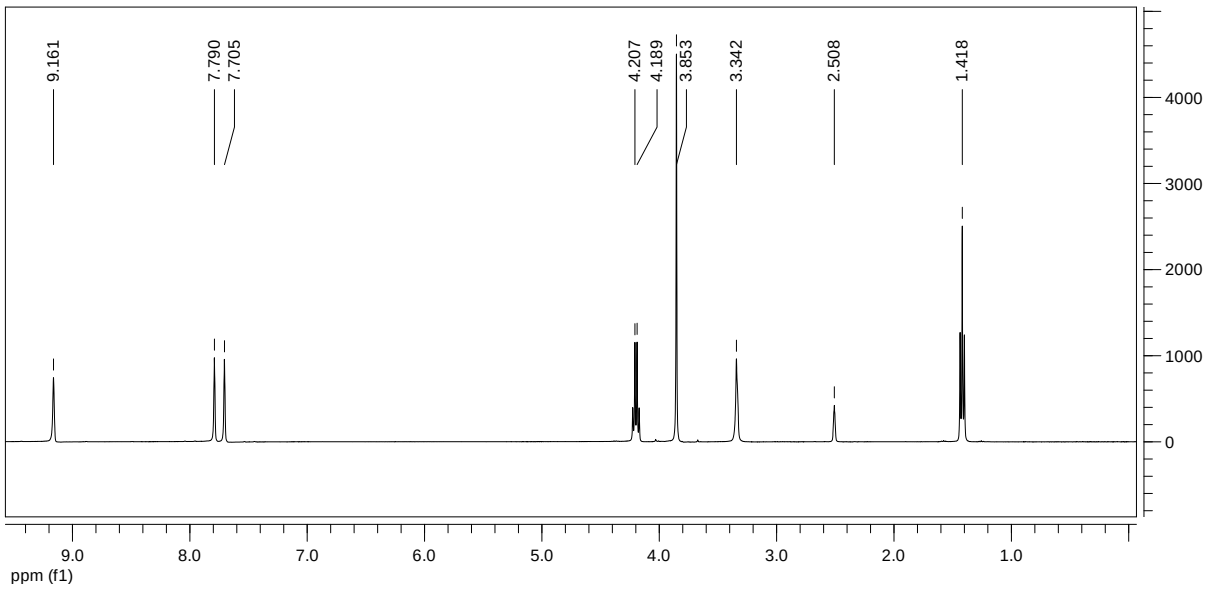

Figure S1. [1]H NMR spectrum of [EMIm][TFSAm].

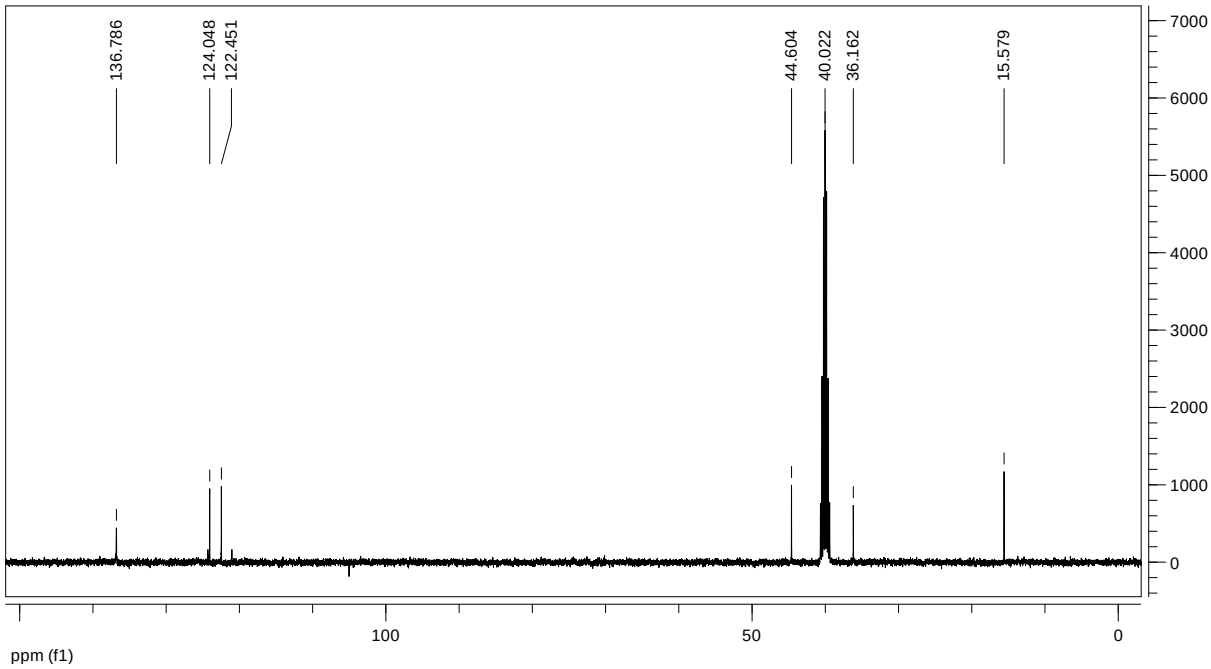

Figure S2. [13]C NMR spectrum of [EMIm][TFSAm].

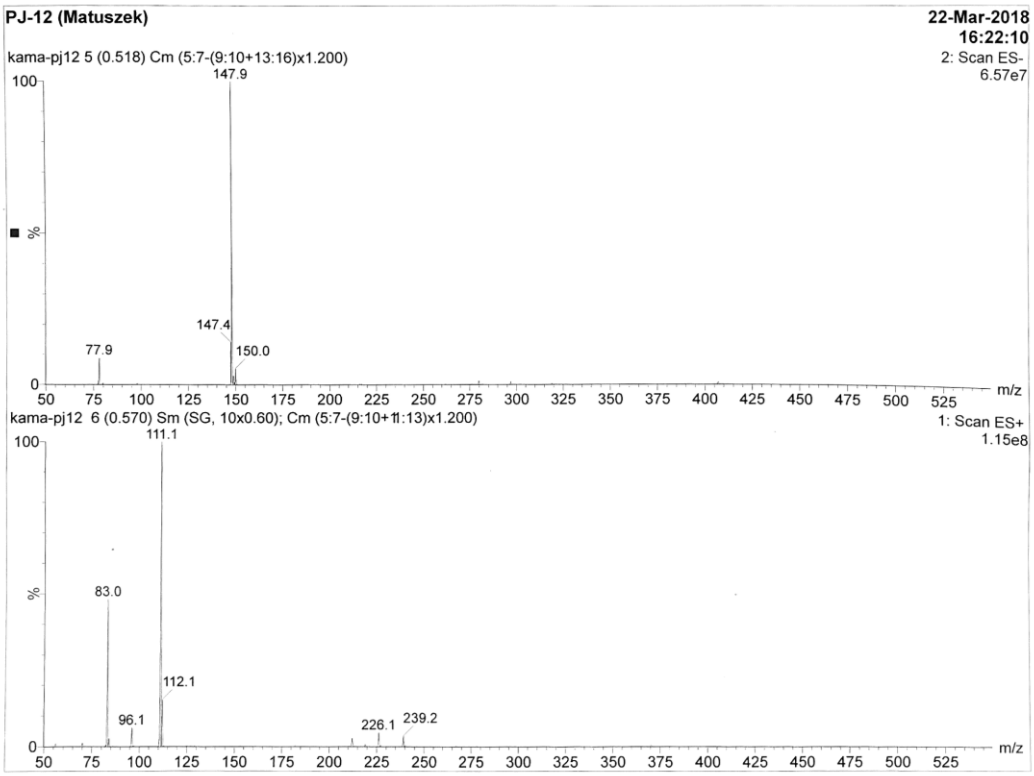

Figure S3. MS spectra of [EMIm][TFSAm].

Table S1. Non-bonding parameters determined for TFSAm

Atom	Charge/e	σ /nm	ε /kJ mol^{-1}
N	-0.70	0.325	0.71128
S	1.00	0.355	1.04600
O1	-0.60	0.296	0.87864
O2	-0.60	0.296	0.87864
F1	-0.20	0.295	0.22175
F2	-0.20	0.295	0.22175
F3	-0.20	0.295	0.22175
H	0.20	0.250	0.12552

Spectroscopic analysis

Increasing the NaTFSI concentration in [EMIm][TFSAm] from x_{NaTFSI}=0.0 to x_{NaTFSI}=0.6 induces shifts in the Raman $\nu_{a\,SO2}$ bands of $[TFSI]^-$ and $[TFSAm]^-$, *ca.* 1340 and 1260 cm^{-1}, respectively (Figure S5); the $[TFSI]^-$ band shifts –9 cm^{-1} and the $[TFSAm]^-$ +12 cm^{-1}, indicating a preference in coordination of Na^+ by $[TFSAm]^-$ (Figure S6). Indeed, the DFT calculation confirms this observation by the higher interaction energies for the $[TFSAm]^-$ containing species (Table S2). Moreover, the most stable complex $[Na(TFSAm)_2]^-$ (Figure S7) contains two anions and thus has a similar structure as has been observed for LiTFSI in [EMIm][TFSI] where a $[Li(TFSI)_2]^-$ complex is formed.[7] The S-N-S/all-breathing band,[8] both present in $[TFSAm]^-$ and $[TFSI]^-$, also changes with NaTFSI concentration. Starting at *ca.* 743 cm^{-1} for the neat AAIL, the band becomes broader with increasing NaTFSI content (Figure S5c). A new contribution at *ca.* 750 cm^{-1} can be ascribed to Na^+-$[TFSAm]^-$ interaction, whereas "free" $[TFSI]^-$ is found at *ca.* 740 cm^{-1} as expected. The latter initially increases in intensity and significantly shifts to 744 cm^{-1} for the highest salt concentration – signifying a much higher level of aggregation also by Na^+.[9] In addition an entirely new band emerges at 762 cm^{-1} – a quite narrow feature which can be related to formation of a crystalline Na_xTFSAm_y phase as also detected by DSC at *ca.* 160 ^oC for two compositions, x_{NaTFSI}=0.50 and x_{NaTFSI}=0.60. An analysis of the $\nu_{S\text{-}N}$ vibration of TFSAm, *ca.* 960-1020 cm^{-1}, shows a broad peak at 978 cm^{-1} in the Raman spectrum at low concentrations (x_{NaTFSI} between 0.0 and 0.15) that disappears upon further salt addition, creating a new narrow signal at 1010 cm^{-1} for the highest concentrations (x_{NaTFSI}=0.5 and x_{NaTFSI}=0.6) (Figure S5b); whereas FTIR analysis of the same spectral range shows an initial feature at 969 cm^{-1}, shifting up to 977 cm^{-1} for x_{NaTFSI} = 0.40 together with increase contribution from two new bands at 996 and 989 cm^{-1} –most pronounced for x_{NaTFSI} = 0.50 and 0.60 (Figure S6c). This change in local structure can possibly explain the increase in ion conductivity at higher salt concentrations with a maximum for x_{NaTFSI} = 0.50. Some more insight is given by an analysis essential for this system's N-H bond, a vibration observable by FTIR spectroscopy at about 3300 cm^{-1}. Starting from x_{NaTFSI}=0.0 the signal at 3279 cm^{-1} shifts towards 3330 cm^{-1} for x_{NaTFSI}=0.3, indicating a weaker intermolecular H-bonding – possibly related to an increasing competition with Na^+ coordination to the oxygen atoms of the anion. Further addition of salt (x_{NaTFSI}>0.4) causes the appearance of two narrow signals at 3284 and 3349 cm^{-1}, indicating two types of [TFSAm] anions inside crystalline Na_xTFSAm_y complexes: with and without H-bonding, respectively.

MD analysis

To further study the molecular level effects of adding NaTFSI to the AAIL – especially targeting the local coordination rather than dynamics, MD simulations were performed. The MD results basically show three types of coordination centres to be active (Figure S8a): the oxygen atoms of both anions (O_{TFSAm} and O_{TFSI}) and the nitrogen atom of $[TFSAm]^-$ (N_{TFSAm}). Hence the MD simulations more or less confirmed the minor contribution of $[TFSI]^-$ in coordinating Na^+, which was inferred above; for the equimolar system $[TFSAm]^-$ contributes more to the 1st solvation shell of Na^+, CN=3.15, than $[TFSI]^-$ does, CN=2.67, despite the former anion having fewer coordination centres. Looking into the details, the contribution from O_{TFSAm} is *ca.* double that of N_{TFSAm} for all systems, indicating a similar coordination ability of these two types of centres. The contribution of both of them decreases when adding more NaTFSI and instead F_{TFSAm} increases, up to Coordination Number equal 0.30 for the most concentrated system, which may indicate some immobilization of [TFSAm] by formation of densely packed Na_xTFSAm_y clusters, seen in the MD simulations as a non-uniform aggregation of [TFSAm] anions (Figure S8b-e). Such an immobilization is observed from analysing the calculated diffusion coefficients, which decrease for both the [TFSAm] and the [TFSI] anions when adding Na-salt, while for the IL cations maxima are observed. Increasing the Na-salt concentration the mobility increases until ca. x_{NaTFSI} = 0.2 with maxima of 13.2 10^{-10} cm^2s^{-1} (Table S3). Upon further addition of Na-salt the mobility decreases

until larger ionic clusters are formed facilitating Na^+ transport, resulting in a second maximum at x_{NaTFSI} = 0.5 with maxima of 6.7 10^{-10} cm^2s^{-1}. A similar trend is observed for the overall mobility, which corresponds to the experimentally observed ionic conductivity maxima at x_{NaTFSI}=0.15 and x_{NaTFSI}=0.5

Figures

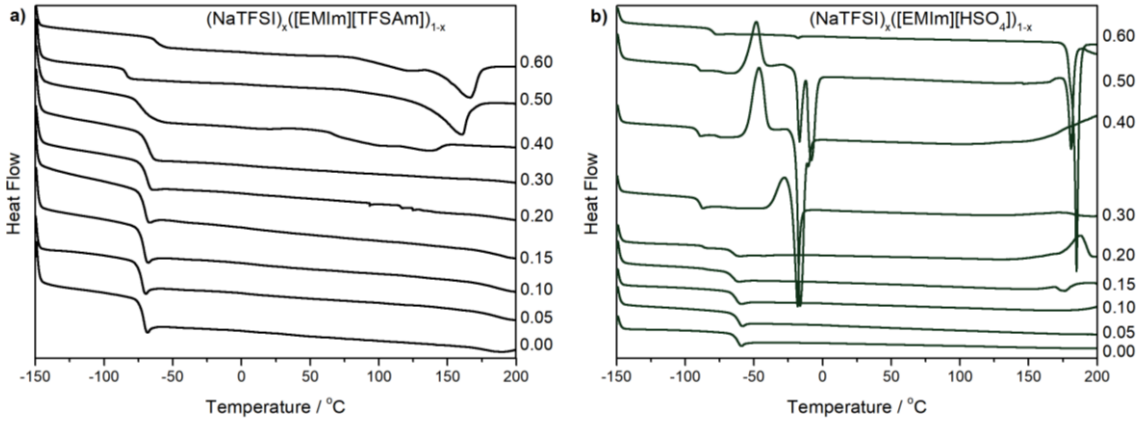

Figure S4. DSC curves corresponding to cooling of $(NaTFSI)_x([EMIm][TFSAm])_{1-x}$ (a) and $(NaTFSI)_x([EMIm][HSO_4])_{1-x}$ (b) samples.

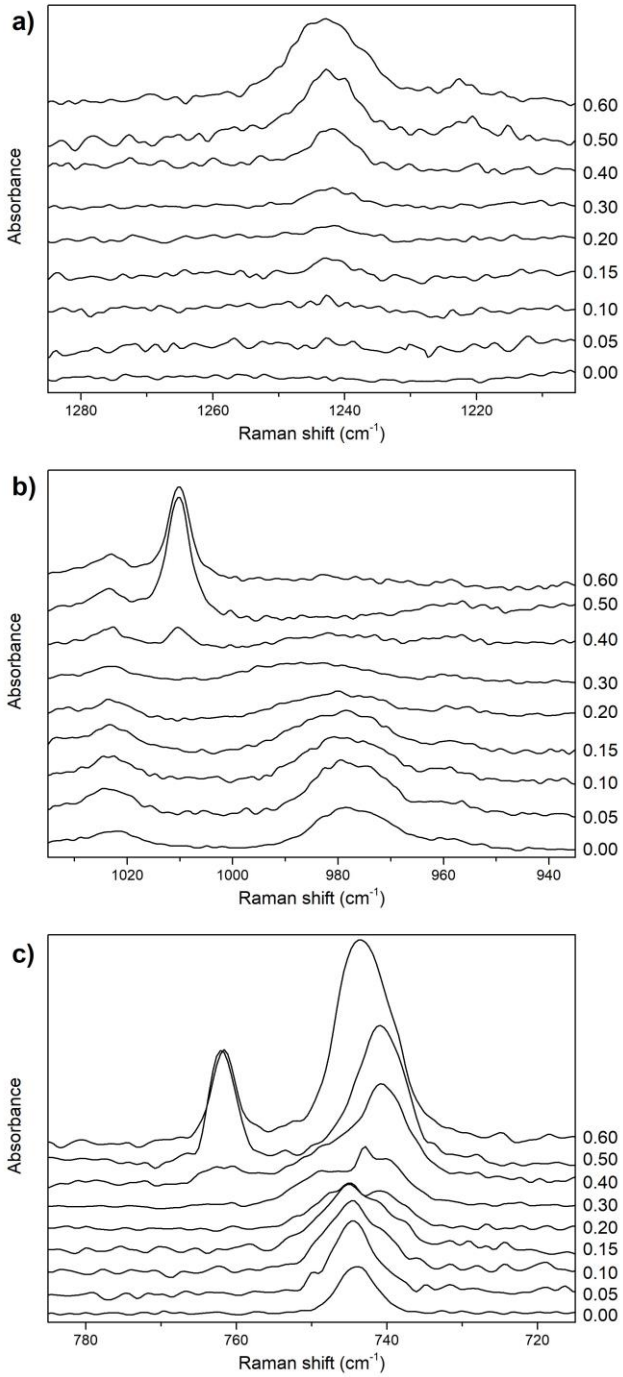

Figure S5. Raman spectra of $(NaTFSI)_x([EMIm][TFSAm])_{1-x}$.

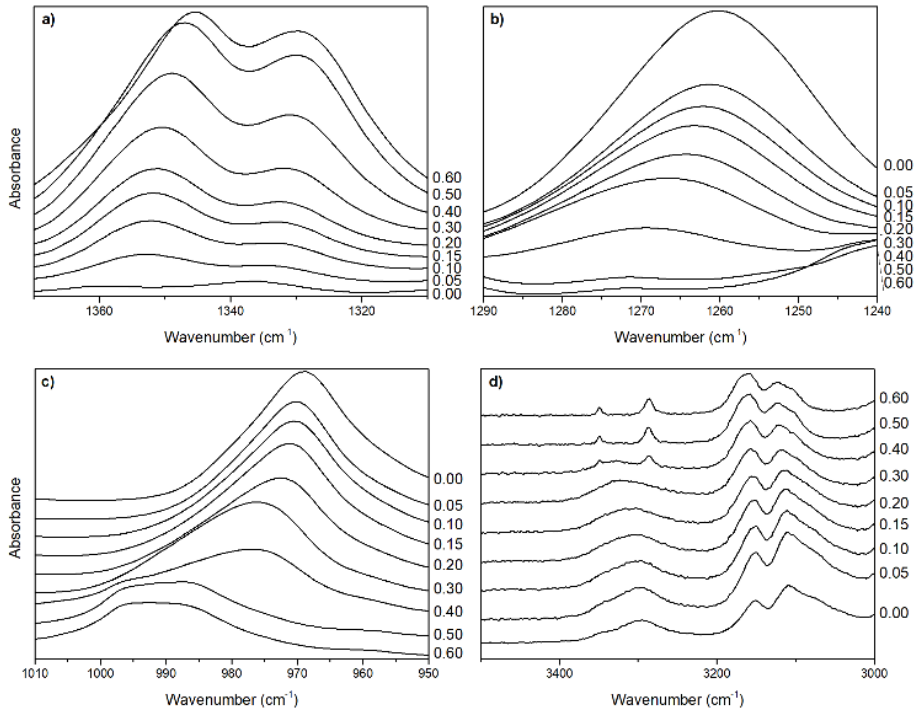

Figure S6. FTIR spectra of electrolytes $(NaTFSI)_x([EMIm][TFSAm])_{1-x}$.

Table S2. DFT-calculated binding energies of $Na(TFSI)_n(TFSAm)_m$ (kJ mol^{-1}).

		n (TFSI)				
		0	**1**	**2**	**3**	**4**
m (TFSAm)	**0**	-	-498.9	-694.5	-611.6	-316.5
	1	-545.2	-721.3	-613.8	-320.8	
	2	-747.7	-615.8	-323.9		
	3	-627.2	-325.6			
	4	-327.6				

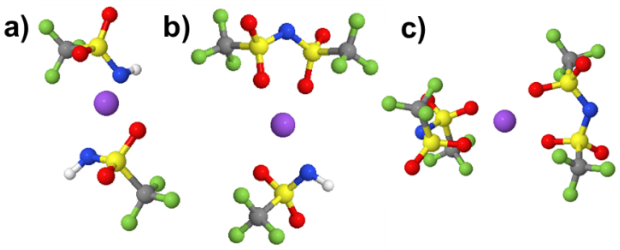

Figure S7.Geometries of the most stable complexes.

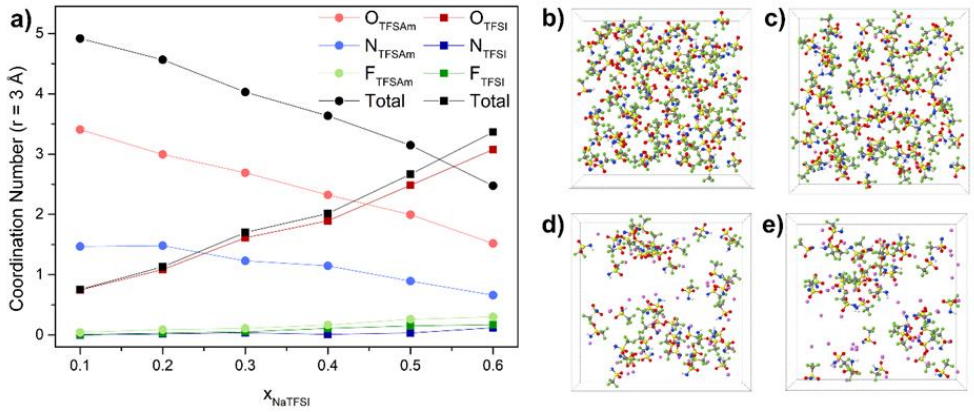

Figure S8. Composition of the 1st solvation shell of Na+ for $(NaTFSI)_x([EMIm][TFSAm])_{1-x}$ as determined from MD simulations (a) and snapshots from the MD simulations (only Na^+ and TFSAm are shown) of $(NaTFSI)_0([EMIm][TFSAm])_1$ (b), $(NaTFSI)_{0.1}([EMIm][TFSAm])_{0.9}$ (c), $(NaTFSI)_{0.5}([EMIm][TFSAm])_{0.5}$ (d), and $(NaTFSI)_{0.6}([EMIm][TFSAm])_{0.4}$(e).

Table S3. Diffusion coefficients and total mobility as a product of diffusion and concentration (all in 10^{-10} cm^2s^{-1}) as obtained from the MD simulations

x_{NaTFSI}	**0.0**	**0.1**	**0.2**	**0.3**	**0.4**	**0.5**	**0.6**
Na^+	-	5.8	13.2	6.9	4.7	6.7	6.0
EMIm	49.6	73.5	26.0	39.1	20.7	27.4	28.2
TFSI	-	35.1	35.8	29.4	21.3	16.2	13.8
TFSAm	27.8	18.1	18.0	17.6	9.4	8.9	8.5

References

1 M. J. Frisch, G. W. Trucks, H. B. Schlegel, G. E. Scuseria, M. A. Robb, J. R. Cheeseman, G. Scalmani, V. Barone, B. Mennucci, G. A. Petersson, H. Nakatsuji, M. Caricato, X. Li, H. P. Hratchian, A. F. Izmaylov, J. Bloino, G. Zheng, J. L. Sonnenberg, M. Hada, M. Ehara, K. Toyota, R. Fukuda, J. Hasegawa, M. Ishida, T. Nakajima, Y. Honda, O. Kitao, H. Nakai, T. Vreven, J. A. Montgomery Jr., J. E. Peralta, F. Ogliaro, M. J. Bearpark, J. Heyd, E. N. Brothers, K. N. Kudin, V. N. Staroverov, R. Kobayashi, J. Normand, K. Raghavachari, A. P. Rendell, J. C. Burant, S. S. Iyengar, J. Tomasi, M. Cossi, N. Rega, N. J. Millam, M. Klene, J. E. Knox, J. B. Cross, V. Bakken, C. Adamo, J. Jaramillo, R. Gomperts, R. E. Stratmann, O. Yazyev, A. J. Austin, R. Cammi, C. Pomelli, J. W. Ochterski, R. L. Martin, K. Morokuma, V. G. Zakrzewski, G. A. Voth, P. Salvador, J. J. Dannenberg, S. Dapprich, A. D. Daniels, Ö. Farkas, J. B. Foresman, J. V. Ortiz, J. Cioslowski and D. J. Fox, *Gaussian 16, Revision B.01*, Gaussian, Inc., Wallingford, CT, USA, 2016.

2 P. Jankowski, W. Wieczorek and P. Johansson, *J. Mol. Model.*, 2017, **23**, 6.

3 M. J. Abraham, T. Murtola, R. Schulz, S. Páll, J. C. Smith, B. Hess and E. Lindahl, *SoftwareX*, 2015, **1–2**, 19–25.

4 W. L. Jorgensen, D. S. Maxwell and J. Tirado-Rives, *J. Am. Chem. Soc.*, 1996, **118**, 11225–11236.

5 T. Köddermann, D. Reith and R. Ludwig, *ChemPhysChem*, 2013, **14**, 3368–3374.

6 J. N. Canongia Lopes, J. Deschamps and A. A. H. Pádua, *J. Phys. Chem. B*, 2004, **108**, 2038–2047.

7 J.-C. Lassègues, J. Grondin, C. Aupetit and P. Johansson, *J. Phys. Chem. A*, 2009, **113**, 305–314.

8 I. Rey, P. Johansson, J. Lindgren, J. C. Lassègues, J. Grondin and L. Servant, *J. Phys. Chem. A*, 1998, **102**, 3249–3258.

9 A. Boschin and P. Johansson, *Electrochimica Acta*, 2015, **175**, 124–133.